

Cooper minimum of high-order harmonic spectra from an MgO crystal in an ultrashort laser pulseYiting Zhao,^{1,2} Xiaoqin Xu,¹ Shicheng Jiang,³ Xi Zhao[⊗],⁴ Jigen Chen[⊗],^{1,*} and Yujun Yang^{2,†}¹Zhejiang Provincial Key Laboratory for Cutting Tools, Taizhou University, Taizhou 31800, China²Institute of Atomic and Molecular Physics, Jilin University, Changchun 130012, China³State Key Laboratory of Precision Spectroscopy, East China Normal University, Shanghai 200062, China⁴Department of Physics, J. R. Macdonald Laboratory, Kansas State University, Manhattan, Kansas 66506, USA

(Received 19 September 2019; accepted 2 March 2020; published 25 March 2020)

Cooper minimum structure of high-order harmonic spectra from atoms or molecules has been extensively studied. In this paper, we demonstrate that the crystal harmonic spectra from an ultrashort midinfrared laser pulse also exhibit the Cooper minimum characteristic. Based on the accurate band dispersion and k -dependent transition dipole moment (TDM) from the first-principles calculations, it can be found that the harmonic spectra from the MgO crystal along the Γ - X direction present a dip structure in the plateau, which is originated from the valley of TDM by examining the distribution of the harmonic intensity at the k space. The Cooper minimum feature in crystal high-order-harmonic generation (HHG) will pave a new way to retrieve the band information of solid materials by using HHG from the ultrashort midinfrared laser pulse.

DOI: [10.1103/PhysRevA.101.033413](https://doi.org/10.1103/PhysRevA.101.033413)**I. INTRODUCTION**

Atoms and molecules irradiated by an intense laser pulse can produce high-order harmonic generation (HHG) [1–5]. Under the influence of the strong laser field, an electron can be ionized from the bound state, and accelerated in the continuum state, finally it can recombine with the ion and give rise to the emission of extreme ultraviolet (XUV) radiation [2,5,6]. The emitted XUV radiation is closely related to the photorecombination, thus, it could encode the structural information on the irradiated target and can be used to study structural features of the target and, in particular, the Cooper minimum [7–9], which corresponds to the nodal structure in the bound-free transition matrix element.

Because of clear signatures, the photoionization spectroscopy has been traditionally used to observe the Cooper minimum. In the process of HHG, the photorecombination is essentially the time inverse of photoionization, therefore, the Cooper minimum should also appear in the harmonic spectra from atoms or molecules. The minimum structure in HHG from atoms or aligned molecules have been extensively investigated in many works [7–13]. Recently, HHG from solids has attracted great interest because of significant applications in attosecond pulse generation and all-optical reconstruction of the band dispersion of solids [14,15]. It has demonstrated theoretically and experimentally that the interband polarization dominates the harmonics above the band gap for MgO, ZnO, and GaAs driven by a midinfrared laser pulse [16–19]. The interband process for solid HHG can be understood by the semiclassical recollision model [16,17,20–24]: The electron first tunneling excitation from the valence band (VB), then the acceleration on the conduction band (CB), finally the electron-hole recombination results in the harmonic photon. Since

the harmonic generation from the interband current depends strongly on the transition dipole moment (TDM) [25–28] of the solid, if there exists a zero in the matrix element between the valence band and the conduction one, analogous to the harmonic spectra from gaseous media, the Cooper minimum structure is expected to appear in the harmonic spectra from solids.

The structure-related minima in solids also have been extensively investigated. By changing the frequency of the driving laser pulse, it can be found that the cross section is very small at certain frequencies, and the minimum value in solid HHG can be achieved by measuring the ionization [29]. Smith *et al.* observed the minimum structure by directly probing the photoelectron spectrum [30]. Recently, M. *et al.* discussed the minima in solid harmonic spectra [31], which is just like Cohen-Fano-type interference minima from the molecular HHG. In this paper, we demonstrated that the harmonic spectrum from MgO in an ultrashort laser pulse has the minimum structure, which is originated from the transition prohibition of two s states of oxygen in the electronic density distribution.

In this paper, based on the accurate band dispersion and k -dependent TDM from the first-principles calculations, we study the feature of HHG from the MgO crystal in an ultrashort midinfrared laser pulse. It is found that the harmonic spectra from TDM by the first-principles theory show a clear dip structure, which almost does not depend on the parameters of the driving laser pulse. Through analyzing the distribution of the harmonic intensity at different crystal momentums, it is clarified that the minimum of TDM leads to the Cooper minimum structure of HHG spectra.

II. THEORY AND MODELS**A. Semiconductor Bloch equations**

Based on the solution of two-band semiconductor Bloch equations (SBEs) [32–34], we investigate the interaction of

*kiddchen@126.com

†yangyj@jlu.edu.cn

an ultrashort midinfrared laser pulse with the MgO crystal. Atomic units are used throughout this article unless stated otherwise. A linearly polarized laser field is propagated along the Γ - X direction of MgO, and the corresponding SBEs [18,35–37] can be read

$$\begin{aligned} \frac{\partial p_{cv}(\mathbf{k}, t)}{\partial t} = & -i[E_c(\mathbf{k}) - E_v(\mathbf{k}) - i/T_2]p_{cv}(\mathbf{k}, t) \\ & + i[\rho_c(\mathbf{k}, t) - \rho_v(\mathbf{k}, t)]\mathbf{F}(t) \cdot \mathbf{D}_{cv}(\mathbf{k}) \\ & + \mathbf{F}(t) \cdot \nabla_{\mathbf{k}} p_{cv}(\mathbf{k}, t), \end{aligned} \quad (1)$$

$$\begin{aligned} \frac{\partial \rho_v(\mathbf{k}, t)}{\partial t} = & -2 \text{Im}[\mathbf{F}(t) \cdot \mathbf{D}_{cv}(\mathbf{k})p_{cv}(\mathbf{k}, t)] \\ & + \mathbf{F}(t) \cdot \nabla_{\mathbf{k}} \rho_v(\mathbf{k}, t) \end{aligned} \quad (2)$$

$$\begin{aligned} \frac{\partial \rho_c(\mathbf{k}, t)}{\partial t} = & 2 \text{Im}[\mathbf{F}(t) \cdot \mathbf{D}_{cv}(\mathbf{k})p_{cv}(\mathbf{k}, t)] \\ & + \mathbf{F}(t) \cdot \nabla_{\mathbf{k}} \rho_c(\mathbf{k}, t). \end{aligned} \quad (3)$$

Here, $E_v(\mathbf{k})$ [$E_c(\mathbf{k})$] is the dispersion of the highest valence (lowest conduction) band contributing to HHG, $\rho_v(\mathbf{k}, t)$ [$\rho_c(\mathbf{k}, t)$] is the population in the corresponding band, $p_{cv}(\mathbf{k}, t)$ and $\mathbf{D}_{cv}(\mathbf{k})$ are the microscopic interband polarization and the transition dipole moment between the conduction and valence bands, respectively. $\mathbf{F}(t) = \hat{\varepsilon}F(t)$ is the laser electric field with a Gaussian envelope, and $\hat{\varepsilon}$ being the polarization direction. T_2 is the interband dephasing time. In this paper, T_2 is set to a quarter cycle of the driving laser and equals 0.67, 1.33, and 2 fs for 800-, 1600-, and 2400-nm laser pulses, respectively.

The intraband current $\mathbf{J}_{\text{intra}}(t)$ because of the motions of the carriers in the bands under a laser pulse is given by

$$\mathbf{J}_{\text{intra}}(t) = \sum_{\lambda=c,v} \int_{\text{BZ}} \mathbf{v}_{\lambda}(\mathbf{k}) \rho_{\lambda}(\mathbf{k}, t) d\mathbf{k}, \quad (4)$$

where $\mathbf{v}_{\lambda}(\mathbf{k}) = \nabla_{\mathbf{k}} E_{\lambda}(\mathbf{k})$ is the group velocity, λ is the band index, and BZ represents the Brillouin zone. The interband polarization $\mathbf{J}_{\text{inter}}(t)$ from the recombination of the electron with the hole can be expressed by

$$\mathbf{J}_{\text{inter}}(t) = \frac{\partial}{\partial t} \int_{\text{BZ}} \mathbf{D}_{cv}(\mathbf{k}) p_{cv}(\mathbf{k}, t) d\mathbf{k} + c.c. \quad (5)$$

In this paper, we are interested in the harmonic spectrum, which is proportional to the absolute square of the projection of the Fourier-transformed total current onto the laser polarization direction,

$$S_{\text{HHG}} \propto \left| \int_{-\infty}^{\infty} [\mathbf{J}_{\text{intra}} + \mathbf{J}_{\text{inter}}] e^{i\omega t} dt \right|^2. \quad (6)$$

B. Band structure and transition dipole moment

The interband and intraband currents depend significantly on the band structure and TDM [16,26]. By using the Vienna *Ab initio* Simulation Package (VASP) code [38,39], accurate k -dependent energy bands and TDM are achieved here. Geometric optimizations of the MgO crystal with symmetry-group $Fm3m$ were performed within generalized gradient approximation in the parametrization of the Perdew-Burke-Ernzerhof functional. The energy cutoff was set to be 400 eV,

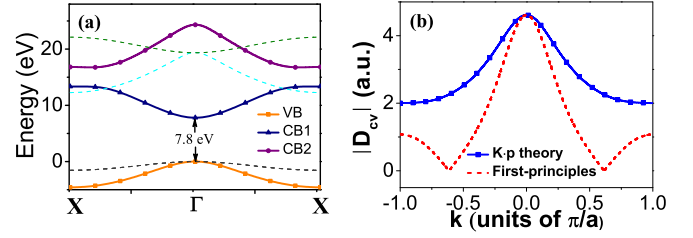


FIG. 1. (a) Band structure of MgO along the Γ - X direction; (b) k -dependent dipole moments between VB and CB1 from the first-principles calculations (dashed red line) and first-order $\mathbf{k} \cdot \mathbf{p}$ theory (solid blue line marked with squares).

and a k -point Monkhorst-Pack mesh of $10 \times 10 \times 10$ was used in the Brillouin zone for electronic structure calculations. Figure 1(a) shows the band structure of MgO along the Γ - X direction, which was calculated by the HSE06 hybrid function with parameter AEXX = 0.43. It can be observed that degenerate heavy-hole and light-hole bands above the split-off one are highest valence bands and the two lowest conduction bands intersect at the boundary of the Brillouin zone. This band dispersion agrees well with the experimental band structure. When the MgO crystal is irradiated by a linearly polarized laser pulse, the harmonic spectra are mainly dominated by three bands marked with VB, CB1, and CB2 in Fig. 1(a) because nonzero transition-matrix elements between them exist in most k points. This characteristic of the band structure along the (001) crystal plane was proved by You *et al.* [40]. Furthermore, the minimum band gap between VB and CB1 is 7.8 eV, which is consistent with the experimental value. The k -dependent TDM can be given by the following two methods where the TDM between the valence band and the conduction one from the first-principles theory can be expressed by:

$$D_{cv}(\mathbf{k}) = \frac{i \langle \Phi_c(\mathbf{k}) | \mathbf{p} | \Phi_v(\mathbf{k}) \rangle}{[E_c(\mathbf{k}) - E_v(\mathbf{k})]}. \quad (7)$$

Because the MgO crystal has inversion symmetry, the TDM between the lowest conduction band and the highest valence band is a real and even function [35] as presented by the red dashed line in Fig. 1(b).

In some of the previous works about solid HHG, the TDM was calculated by the first-order $\mathbf{k} \cdot \mathbf{p}$ theory [26],

$$D_{cv}(\mathbf{k}) = \frac{id_0[\varepsilon_c(0) - \varepsilon_v(0)]}{[E_c(\mathbf{k}) - E_v(\mathbf{k})]}, \quad (8)$$

which is valid when the carriers in conduction or valence bands are mostly populated at Γ . However, under the interaction of a strong laser pulse, electrons (holes) may travel through the entire Brillouin zone, thus, the TDM from the first-order $\mathbf{k} \cdot \mathbf{p}$ approximation is not applicable to this situation. For comparison, the TDM from the first-order $\mathbf{k} \cdot \mathbf{p}$ theory is also shown by the solid blue line marked with squares in Fig. 1(b). Obviously, in the TDM in the first-principles case, there exist minima at $k = \pm 0.6\pi/a$ ($a = 4.213 \text{ \AA}$) and valley structures. Based on the first-principles calculations using the VASP code, we can obtain the electronic density distribution in real space at different k points. Figure 2 presents electronic density distributions of valence and conduction bands at $k =$

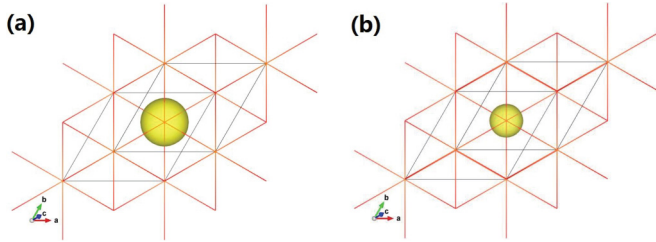


FIG. 2. Electronic density distributions from (a) the valence band and (b) the conduction band at $k = 0.6\pi/a$.

$0.6\pi/a$. It can be seen that electronic density distributions in valence and conduction bands at this k point are mainly derived from the s orbit of oxygen, and the symmetry is the same for these two s states. Thereby the transition probability between these two orbits is very small, which leads to the minimum structure in the k -dependent TDM from the first-principles calculation. Yu *et al.* proved that the shape of the k -dependent TDM plays an important role in harmonic generation [26]. Therefore, we will discuss how the difference in shapes of TDMs effects the HHG spectra.

III. COOPER MINIMUM STRUCTURE OF CRYSTAL HHG

In terms of two-band and three-band SBEs, we first examine the dependence of crystal HHG spectra from the first-principles-based calculations on the driving laser intensity as shown in Figs. 3(a) and 3(b), respectively. Here, the 3-fs/1600-nm midinfrared laser pulse with the CEP 0 is chosen, and the corresponding peak intensity inside the crystal is changed from 5.0×10^{12} to 4.0×10^{13} W/cm². One can see that, as the increase in the laser intensity, HHG spectra in both cases are almost same and the harmonic efficiency is gradually enhanced; when the peak intensity of the laser pulse is stronger than 1.5×10^{13} W/cm², the harmonic spectra from the three-band model appear to be a clear two-plateau structure. In particular, harmonic spectra from the two cases exhibit an apparent minimum near 16 eV in the first plateau. In the following, for better explaining the origin of the dip structure, we focus on harmonic spectra from the two-band SBEs.

Based on the real TDM from the first-principles calculations, the red solid line marked with circles, the black solid line marked with triangles, and the green solid line marked

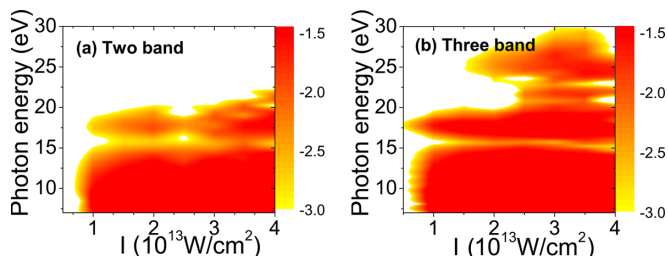


FIG. 3. Dependence of crystal HHG spectra from the (a) two-band and (b) three-band models on the driving laser intensity. The duration, wavelength, and the carrier envelope phase (CEP) of the driving laser pulse are 3 fs, 1600 nm, and 0, respectively.

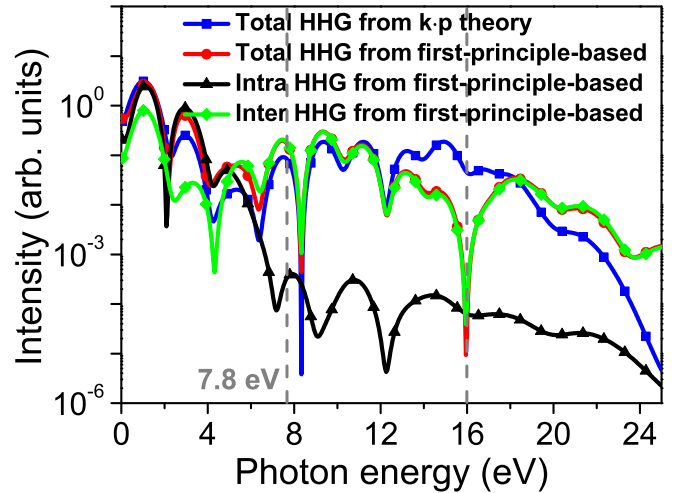


FIG. 4. Harmonic spectra of MgO from TDMs calculated by first-principles (red solid line marked with circles) and first-order $\mathbf{k} \cdot \mathbf{p}$ theories (blue solid line marked with squares); the black solid line marked with triangles and the green solid line marked with rhombuses are harmonic spectra produced by intraband and interband currents from TDM with the first-principles calculations, respectively. The laser peak intensity is 3.0×10^{13} W/cm², and the other laser parameters are the same as in Fig. 3.

with rhombuses in Fig. 4 present harmonic spectra of the MgO crystal in the ultrashort laser pulse, which are generated by the total current, intraband current, and the interband polarization, respectively. The laser peak intensity of the incident laser pulse is 3.0×10^{13} W/cm² (about 1.5 V/Å), which is lower than the damage threshold of MgO.

It is clear that harmonics below and above the band gap are dominated by intraband and interband currents, which agree with the recent results for ZnO, MgO, and GaAs in midinfrared laser pulses [20,40–43]. Figure 4 also shows the harmonic spectrum (blue solid line marked with squares) from the TDM based on the first-order $\mathbf{k} \cdot \mathbf{p}$ theory. Although the first-order $\mathbf{k} \cdot \mathbf{p}$ theory is unreasonable under this laser field parameter, the harmonic spectrum from the first-order $\mathbf{k} \cdot \mathbf{p}$ theory still has a comparative significance. In this case, intensities of harmonics in the plateau are almost same. However, for the spectrum based on the first-principles-based calculations, there exists an obvious minimum structure when the photon energy is 16 eV. This distinction in both cases indicates that the TDM's shape has a significant effect on the crystal harmonic spectra.

Next, we check the influence of laser parameters to the dip structure in harmonic spectra from the real TDM based on the first-principles calculations. Figures 5(a)–5(d) show the HHG spectra of the MgO crystal in laser pulses with different intensities, wavelengths, durations, and CEPs, respectively. It is found that the minimum structure at harmonic spectra is almost independent of parameters of the driving laser pulses. Because harmonics in the plateau are mainly originated from the interband polarization, it is natural to deduce that the dip structure is related to the characteristic of the real TDM of the MgO crystal. In the following, for intuitively clarifying the minimum feature, we focus on the HHG spectrum

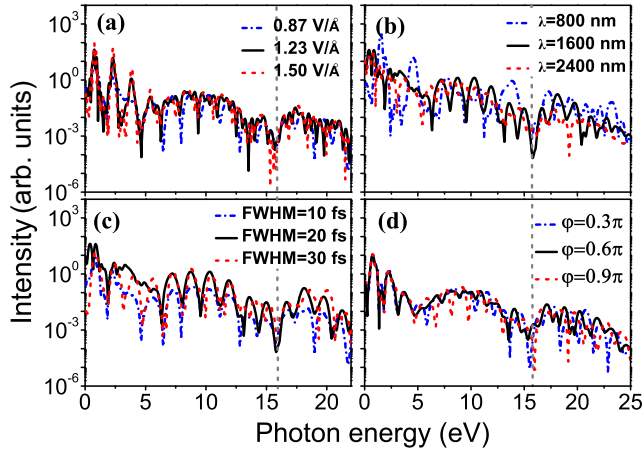


FIG. 5. Harmonic spectra from the real TDM by using first-principles calculations in different laser pulses. (a) The duration, wavelength, and CEP are 10 fs, 1600 nm, and 0, respectively; (b) the duration, peak intensity, and CEP are 10 fs, 2.0×10^{13} W/cm², and 0, respectively; (c) the intensity, wavelength, and CEP are 2.0×10^{13} W/cm², 1600 nm, and 0, respectively; (d) the intensity, wavelength and duration are 2.0×10^{13} W/cm², 1600 nm, and 10 fs, respectively.

from the ultrashort laser pulse as shown by the red solid line marked with circles in Fig. 4.

In order to further understand the emission process in crystal HHG, time-frequency analyses of the harmonic spectra for first-principles-based and first-order $\mathbf{k} \cdot \mathbf{p}$ theory cases are presented in Figs. 6(a) and 6(b). In both cases, time-frequency diagrams of HHG are similar, harmonics beyond the band gap are primarily caused by one quantum path. This result is further confirmed by the harmonic photon energy vs the emission instant calculated from the semiclassical recollision model as shown in the black circle curve from Fig. 6. It means that the harmonic photon above the band gap and the crystal momentum at the emission instant has a one-to-one correspondence in the ultrashort laser pulse. Furthermore, the time-frequency distribution in Fig. 6(a) shows one hole at the photon energy with 16 eV, which directly corresponds to the dip in the harmonic spectrum (the red solid line marked with circles) in Fig. 4. In contrast to the first-principles-based case, there is no hole at 16 eV in the HHG time-frequency distribution from the first-order $\mathbf{k} \cdot \mathbf{p}$ theory as shown in

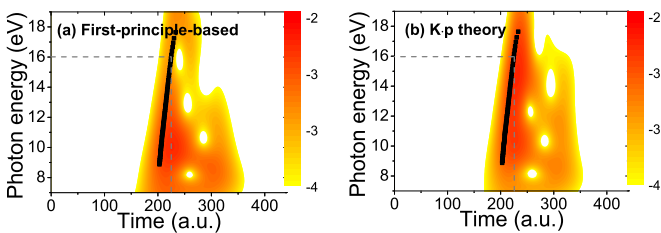


FIG. 6. Time-frequency distributions of the HHG corresponding to (a) the red solid line marked with circles and (b) the blue solid line marked with squares curves in Fig. 4. The black circle curve is the photon energy vs the emission time from the semiclassical recollision model. The laser parameters are the same as in Fig. 4.

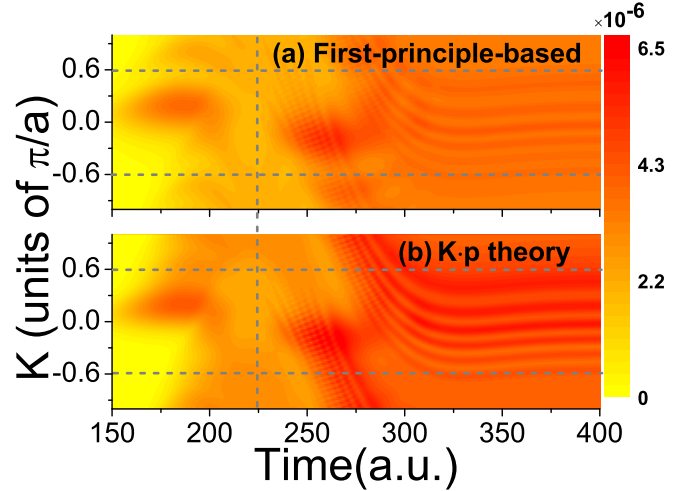


FIG. 7. Electronic populations of the conduction bands for the dipole moments from (a) first-principles and (b) first first-order $\mathbf{k} \cdot \mathbf{p}$ calculations, respectively.

Fig. 6(b). The above results further testify that the minimum structure of the harmonic spectrum is closely concerned with the TDM of the crystal.

The efficiency of HHG from the interband current is proportional to the population of the electron (hole) and the TDM between conduction and valence bands at the recombination time t_r . It can be observed that the emission instant is 225 a.u. from Fig. 6 when the energy of the harmonic photon is equal to 16 eV. To clearly address the physics of the dip structure in harmonic spectra, we examine populations of electrons in the conduction band at this emission instant. Figure 7 shows electronic populations of the conduction band for the first-principles-based and first-order $\mathbf{k} \cdot \mathbf{p}$ cases, respectively. From Figs. 1(a) and 1(b), one can find that the band gap between two bands is exactly equal to 16 eV for the crystal momentum at $k = \pm 0.6\pi/a$. In Fig. 7, populations at these crystal momenta for the emission's instant 225 a.u. are marked by the cross of dashed lines. For both cases, populations at $k = \pm 0.6\pi/a$ with $t_r = 225$ a.u. are no essential difference. This means that the dip structure of the HHG spectrum is almost independent of the electronic population at the recombination instant.

Now that we know the dip structure of the harmonic spectrum is related to the k -dependent TDM, the contribution

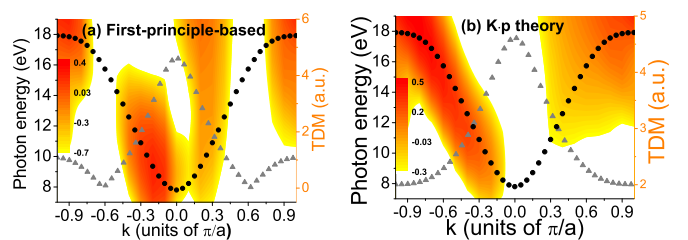


FIG. 8. The contribution of different crystal momenta to harmonics based on the (a) first-principles-based calculations and (b) first first-order $\mathbf{k} \cdot \mathbf{p}$, respectively. The gray triangular curves are the TDMs from the two cases, and the black square curve is the band gap between two bands. The laser parameters are the same as in Fig. 4.

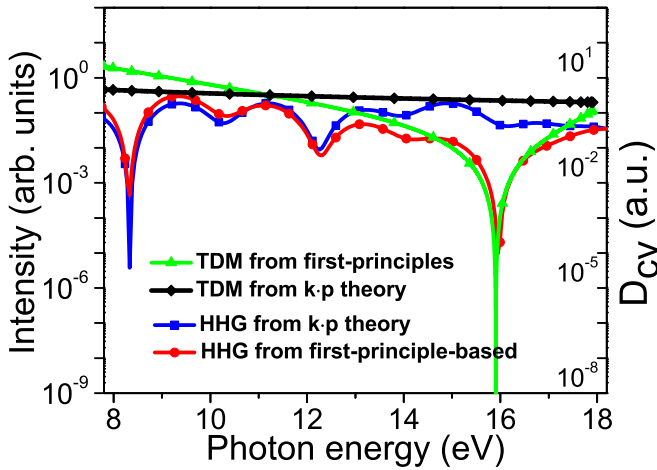


FIG. 9. Values of TDMs from the first-principles calculations (green solid line marked with triangles) and the first-order $\mathbf{k} \cdot \mathbf{p}$ theory (black solid line marked with rhombuses) vs the band gap, and the corresponding harmonic spectra shown by red solid curve marked with circles and blue solid curve marked with squares in Fig. 4.

from different crystal momenta to harmonics above the band gap should be analyzed. Figures 8(b) and 8(a) provide a comparison between distributions of harmonic intensities at different k 's from the first first-order $\mathbf{k} \cdot \mathbf{p}$ theory and first-principles-based calculations, respectively. Here, in order to distinctly reveal distributions of harmonics intensities, we focus on harmonics produced at the main emission times from 200 to 250 a.u.. In the case of the real TDM from the first-principles calculations, the amplitude value of TDM near $k = \pm 0.6\pi/a$ is close to zero as shown by the gray triangular curve in Fig. 8(a), which results in no distribution of the harmonic intensity, as presented in Fig. 8(a). In the first-order $\mathbf{k} \cdot \mathbf{p}$ theory case, TDM has bigger values near $k = \pm 0.6\pi/a$, which induces a clear distribution of the harmonic intensity as observed from Fig. 8(b). Above all, it can be demonstrated that the valley shape of the TDM from the first-principles calculations results in the dip structure in the harmonic spectra.

Finally, we explore dependences of amplitudes of TDMs from the first-principles calculations and the first-order $\mathbf{k} \cdot \mathbf{p}$ theory with the band gap as shown by the green solid line marked with triangles and black solid line marked with rhombuses in Fig. 9. The corresponding harmonic spectra in both cases are also presented in Fig. 9. In the case of the first-order $\mathbf{k} \cdot \mathbf{p}$ theory, TDM and the harmonic spectrum near 16 eV have no minimum structures. However, for the case

of the first-principles-based calculations, the TDM's valley at 16 eV directly coincides with the minimum of the harmonic spectrum. Thereby we can draw a conclusion that, because in the amplitude of TDM between valence and conduction bands there exists zero values, harmonic spectra from the MgO crystal also exhibit the Cooper minimum structure, which is similar to harmonic spectra from gaseous media.

IV. SUMMARY

In conclusion, we have demonstrated that harmonic spectra of the MgO crystal in the ultrashort laser pulse have the Cooper minimum structure. By comparing harmonic spectra from TDMs of the first-order $\mathbf{k} \cdot \mathbf{p}$ theory and the first-principles calculations, it is confirmed that the shape of the TDM plays an important role in the generation of the HHG spectrum, and the valley of the real TDM from the first-principles calculations lead to the dip structure near 16 eV in the harmonic spectra from the MgO crystal. More importantly, by taking the valley-dip correspondence as the benchmark, the emitted photon energy and the crystal momentum have a one-to-one match, and the intensity of the harmonic from an ultrashort laser pulse is approximately proportional to the square of the TDM's value. Thereby the k -dependent band gap and TDM between valence and conduction bands are hoped to be mapped by harmonics with energies above the minimum band gap, which will pave a new way to the all-optical reconstruction of the electronic band structure by taking advantage of the crystal HHG.

ACKNOWLEDGMENTS

The authors sincerely thank Prof. R. Lu for providing the code. J. Chen was supported by the National Natural Science Foundation of China under Grant No. 11975012 and the Outstanding Youth Project of Taizhou University (Grant No. 2019JQ002). Project supported by the National Key Research and Development Program of China (Grants No. 2019YFA0307700 and No. 2017YFA0403300), the National Natural Science Foundation of China (Grants No. 11774129 and No. 11627807), the Jilin Provincial Research Foundation for Basic Research, China (Grant No. 20170101153JC), and the Science and Technology Project of the Jilin Provincial Education Department (Grant No. JJKH20190183KJ). And we acknowledge the High Performance Computing Center of Jilin University for supercomputer time.

- [1] A. McPherson, G. Gibson, H. Jara, U. Johann, T. S. Luk, I. A. McIntyre, K. Boyer, and C. K. Rhodes, *J. Opt. Soc. Am. B* **4**, 595 (1987).
- [2] M. Lewenstein, P. Balcou, M. Y. Ivanov, A. L'Huillier, and P. B. Corkum, *Phys. Rev. A* **49**, 2117 (1994).
- [3] A. L'Huillier and P. Balcou, *Phys. Rev. Lett.* **70**, 774 (1993).
- [4] T. Brabec and F. Krausz, *Rev. Mod. Phys.* **72**, 545 (2000).
- [5] F. Krausz and M. Ivanov, *Rev. Mod. Phys.* **81**, 163 (2009).

- [6] P. B. Corkum, *Phys. Rev. Lett.* **71**, 1994 (1993).
- [7] S. B. Schoun, R. Chirila, J. Wheeler, C. Roedig, P. Agostini, L. F. DiMauro, K. J. Schafer, and M. B. Gaarde, *Phys. Rev. Lett.* **112**, 153001 (2014).
- [8] J. G. Chen, Y. J. Yang, J. Chen, and B. B. Wang, *Phys. Rev. A* **91**, 043403 (2015).
- [9] F. Cloux, B. Fabre, and B. Pons, *Phys. Rev. A* **91**, 023415 (2015).

- [10] J. P. Farrell, L. S. Spector, B. K. McFarland, P. H. Bucksbaum, M. Gühr, M. B. Gaarde, and K. J. Schafer, *Phys. Rev. A* **83**, 023420 (2011).
- [11] J. Higuete, H. Ruf, N. Thiré, R. Cireasa, E. Constant, E. Cormier, D. Descamps, E. Mével, S. Petit, B. Pons, Y. Mairesse, and B. Fabre, *Phys. Rev. A* **83**, 053401 (2011).
- [12] J. Higuete *et al.*, *J. Phys.: Conf. Ser.* **388**, 022023 (2012).
- [13] M. C. H. Wong, A. T. Le, A. F. Alharbi, A. E. Boguslavskiy, R. R. Lucchese, J. P. Brichta, C. D. Lin, and V. R. Bhardwaj, *Phys. Rev. Lett.* **110**, 033006 (2013).
- [14] G. Vampa, T. J. Hammond, N. Thiré, B. E. Schmidt, F. Légaré, C. R. McDonald, T. Brabec, D. D. Klug, and P. B. Corkum, *Phys. Rev. Lett.* **115**, 193603 (2015).
- [15] V. Venkataraman, K. Saha, P. Londero, and A. L. Gaeta, *Phys. Rev. Lett.* **107**, 193902 (2011).
- [16] S. Ghimire, A. D. DiChiara, E. Sistrunk, P. Agostini, L. F. DiMauro, and D. A. Reis, *Nat. Phys.* **7**, 138 (2011).
- [17] G. Vampa, C. R. McDonald, G. Orlando, D. D. Klug, P. B. Corkum, and T. Brabec, *Phys. Rev. Lett.* **113**, 073901 (2014).
- [18] M. Wu, S. Ghimire, D. A. Reis, K. J. Schafer, and M. B. Gaarde, *Phys. Rev. A* **91**, 043839 (2015).
- [19] G. Vampa, T. J. Hammond, N. Thiré, B. E. Schmidt, F. Légaré, C. R. McDonald, T. Brabec, and P. B. Corkum, *Nature (London)* **522**, 462 (2015).
- [20] G. Vampa, C. R. McDonald, G. Orlando, P. B. Corkum, and T. Brabec, *Phys. Rev. B* **91**, 064302 (2015).
- [21] S. A. Sørngård, S. I. Simonsen and J. P. Hansen, *Phys. Rev. A* **87**, 053803 (2013).
- [22] D. Dimitrovski, T. G. Pedersen, and L. B. Madsen, *Phys. Rev. A* **95**, 063420 (2017).
- [23] G. Vampa, C. McDonald, A. Fraser, and T. Brabec, *IEEE J. Sel. Top. Quant.* **21**, 1 (2015).
- [24] S. C. Jiang, C. Yu, G. L. Yuan, T. Wu, Z. W. Wang, and R. F. Lu, *J. Phys.: Condens. Matter* **29**, 275702 (2017).
- [25] M. S. Wismer, S. Y. Kruchinin, M. Ciappina, M. I. Stockman, and V. S. Yakovlev, *Phys. Rev. Lett.* **116**, 197401 (2016).
- [26] C. Yu, X. Zhang, S. Jiang, X. Cao, G. Yuan, T. Wu, L. Bai, and R. Lu, *Phys. Rev. A* **94**, 013846 (2016).
- [27] S. C. Jiang, J. G. Chen, H. Wei, C. Yu, R. F. Lu, and C. D. Lin, *Phys. Rev. Lett.* **120**, 253201 (2018).
- [28] Y. T. Zhao, S. Y. Ma, S. C. Jiang, Y. J. Yang, X. Zhao, and J. G. Chen, *Opt. Express* **27**, 34392 (2019).
- [29] I. Abbati, L. Braicovich, G. Rossi, I. Lindau, U. del Pennino, and S. Nannarone, *Phys. Rev. Lett.* **50**, 1799 (1983).
- [30] D. R. Smith, W. J. Padilla, D. C. Vier, S. C. Nemat-Nasser, and S. Schultz, *Phys. Rev. Lett.* **84**, 4184 (2000).
- [31] Mrudul M. S., A. Pattanayak, M. Ivanov, and G. Dixit, *Phys. Rev. A* **100**, 043420 (2019).
- [32] P. Földi, M. G. Benedict, and V. S. Yakovlev, *New J. Phys.* **15**, 063019 (2013).
- [33] D. Golde, T. Meier, and S. W. Koch, *J. Opt. Soc. Am. B* **23**, 2559 (2006).
- [34] D. Golde, M. Kira, T. Meier, and S. W. Koch, *Phys. Status Solidi B* **248**, 863 (2011).
- [35] S. Jiang, H. Wei, J. Chen, C. Yu, R. Lu, and C. D. Lin, *Phys. Rev. A* **96**, 053850 (2017).
- [36] T. T. Luu and H. J. Wörner, *Phys. Rev. B* **94**, 115164 (2016).
- [37] C. Yu, S. Jiang, T. Wu, G. L. Yuan, Z. W. Wang, C. Jin, and R. F. Lu, *Phys. Rev. B* **98**, 085439 (2018).
- [38] G. Kresse and J. Furthmüller, *Phys. Rev. B* **54**, 11169 (1996).
- [39] J. P. Perdew, K. Burke, and M. Ernzerhof, *Phys. Rev. Lett.* **77**, 3865 (1996).
- [40] Y. S. You, M. X. Wu, Y. C. Yin, A. Chew, X. M. Ren, S. G. Mirzaei, D. A. Browne, M. Chini, Z. H. Chang, K. J. Schafer, M. B. Gaarde, and S. Ghimire, *Opt. Lett.* **42**, 1816 (2017).
- [41] D. Golde, T. Meier, and S. W. Koch, *Phys. Rev. B* **77**, 075330 (2008).
- [42] Z. Wang, H. Park, Y. H. Lai, J. L. Xu, C. I. Blaga, F. Y. Yang, P. Agostini, and L. F. DiMauro, *Nat. Commun.* **8**, 1686 (2017).
- [43] M. X. Wu, D. A. Browne, K. J. Schafer, and M. B. Gaarde, *Phys. Rev. A* **94**, 063403 (2016).